Dynamical Analysis of Mpox Transmission Model Incorporating Asymptomatic Individuals

Tuhfatul Janan[1,2], Fatmawati[1,*], Agus Hasan[3]

[1]Department of Mathematics, Faculty of Science and Technology, Universitas Airlangga, Surabaya 60115, Indonesia
[2]Department of Mathematics Education, Faculty of Education and Teacher Training, Institut Ahmad Dahlan Probolinggo, Probolinggo 67231, Indonesia
[3]Department of ICT and Natural Sciences, Norwegian University of Science and Technology, Alesund 6025, Norway

*Email: fatmawati@fst.unair.ac.id

Abstract

In this paper, we develop a mathematical model for the transmission dynamics of monkeypox (Mpox) involving both human and rodent populations, with the human population including asymptomatic individuals. The analysis begins by establishing the well-posedness of the model using the contraction mapping principle, ensuring the existence, uniqueness, and stability of the solution. The model is further examined for the boundedness and non-negativity of the solutions. Three equilibrium points are identified: the disease-free equilibrium, the human-endemic equilibrium, and the endemic equilibrium. The disease-free equilibrium is shown to be both locally and globally asymptotically stable when the basic reproduction number is less than one. If they exist, the human-endemic equilibrium is proven to be globally asymptotically stable when the basic reproduction number of the rodent population is less than one, and the endemic equilibrium is always globally asymptotically stable. The sensitivity analysis indicates that vaccination and contact dynamics are the most influential factors in human transmission, while rodent transmission is primarily shaped by contact rates and mortality-related factors. Numerical simulations are provided to illustrate and validate the analytical results.

Keywords: Infectious disease, Mpox, mathematical model, asymptomatic, stability
2010 MSC classification number: 00A71, 37N25, 81T80, 93A30

1. INTRODUCTION

Monkeypox (Mpox) is a zoonotic viral infection caused by the Mpox virus, a member of the Orthopoxvirus genus, which is in the same group as the variola virus that causes smallpox [14]. The virus is divided into two major clades: Clade I, which represents subclades Ia and Ib, and Clade II, which includes subclades IIa and IIb. These vary in their geographic distribution and virulence profiles. The first isolation was from monkeys in Denmark in 1958. Later, in 1970, the first human case was identified in the Democratic Republic of Congo [40]. Since then, Mpox has become endemic in many parts of Central and West Africa, with only scattered outbreaks linked to animal-to-human transmission events. However, in May 2022, the disease began its resurgence worldwide, extending to regions outside Africa's endemic areas reaching Europe and North America, which was driven primarily by international travel and close human-to-human contact [39]. In view of its unprecedented geographical spread, the World Health Organization (WHO) declared Mpox a Public Health Emergency of International Concern (PHEIC) on August 14, 2024, after having verified more than 100,000 cases and 220 deaths in 120 countries worldwide [42].

Transmission of Mpox occurs via multiple routes involving both zoonotic and human-to-human pathways. Direct contact with infected persons, animals, or contaminated materials facilitates the spread of the virus [15]. Human transmission primarily occurs via respiratory droplets, exposure to skin or mucosal lesions, and contact with bodily fluids [35], while vertical transmission from mother to fetus or newborn has also been suggested. Zoonotic infection is typically associated with exposure to fluids, bites, or scratches from infected

*Corresponding Author
Received November 3^{rd}, 2025, Revised February 15^{th}, 2026, Accepted for publication April 7^{th}, 2026. e-ISSN: 2549-2896, DOI:10.5614/cbms.2026.9.1.4

wild animals during hunting or food preparation activities [5], [15], [40]. Additionally, fomite transmission through contaminated surfaces such as bedding, clothing, or medical equipment remains a potential source of infection in both community and healthcare settings [15]. The Mpox incubation period ranges from 6 to 13 days and may extend to 21 days [37], [38]. Symptoms such as rash, fever, fatigue, and lymphadenopathy usually last 2–4 weeks and resolve with supportive care. Severe cases occur mainly in newborns, children, pregnant women, and immunocompromised individuals, with a reported case fatality rate of 0.1–10% [41].

Mathematical modeling serves as a powerful tool to guide appropriate interventions and deepen understanding of infectious disease dynamics and control [25],[27]. Classical compartmental models, which include susceptible, infected, and recovered subpopulations, have laid the foundation for more complex disease modeling. These models have been extended to incorporate additional subpopulations, such as vaccinated and asymptomatic individuals, to better reflect public health scenarios. Incorporating such compartments improves the ability of models to evaluate intervention strategies. Al-Shomrani et al. [6] demonstrated that models that combine these subpopulations have better predictions for the effectiveness of public health interventions in mitigating the spread of diseases. In another related context, Abidemi et al. [1] proposed a deterministic double-dose vaccination model for COVID-19 transmission and demonstrated how this might be subjected to optimum control and cost-effectiveness analysis in determining vaccination policy. Similar multi-disease models have been adopted to study the interactions between the diseases, including the dynamics of co-infection of COVID-19 and dengue [9], pointing out the wide applicability of mathematical models in epidemiology. Recent studies on the modeling of infectious disease can be found in [3], [17], [28], [29].

Several models for Mpox transmission consider both human and rodent populations, while a vaccinated human sub-population has also received considerable attention from several authors. Elsonbaty et al. [19] highlighted vaccination as an important measure that will enhance herd immunity and subsequently reduce disease susceptibility. Afolabi and Wade [2] presented evidence that imperfect vaccines add to disease mitigation. These studies further highlight the role played by improving vaccine efficacy and continuously adapting disease control policies as epidemiological and vaccination dynamics evolve. Sayarshad [34] used data from the United States to show that with coordination, vaccine coverage increased by 35%, while unmet demand fell by 60%, compared to individual manufacturer-based approaches. Other studies incorporating a vaccinated human sub-population have been conducted by Akinyemi et al. [4], Bankuru et al. [7], Olaniyi and Chuma [31], and Samreen et al. [33].

According to WHO, asymptomatic individuals infected with Mpox can indeed spread the virus without developing symptoms [40]. Li et al. [23] extended a model that incorporated asymptomatic humans into it, making the model more realistic as far as disease transmission dynamics are concerned. Their numerical simulations and dynamic analysis determined that asymptomatic humans can contribute much toward the spreading infection and, therefore, could be included in controls like vaccination and personal protection. Similarly, Fernandes and Maldonado [20] determined that asymptomatic people have no symptoms but can transfer the virus through sexual contact and are thus crucial for determining the disease's transmission rate. This work provides important insights for public health authorities on the assessment of preventive measures and in designing control strategies, particularly those involving sexually transmissible diseases with asymptomatic transmission. Further works related to mathematical modeling of Mpox transmission, not reviewed in the above, are listed in the following references [8], [10], [13], [21], [30], [43].

In this paper, we propose a mathematical model for the transmission of Mpox, incorporating an asymptomatic human subpopulation combined with a vaccinated human subpopulation. Unlike other available Mpox transmission models that concentrate on symptomatic infections, our model accounts for the hidden potential of Mpox transmission through asymptomatic infections, as well as vaccination-induced immunity. This dual account of Mpox infections provides a more realistic view of Mpox epidemiology. The novelty of this paper lies not only in the integrated human–rodent transmission structure but also in the rigorous analytical framework applied to the model. First, the contraction mapping principle is used to establish the well-posedness, which guarantees the existence, uniqueness, and stability of the solution, an approach that is rarely explored in epidemiological modeling studies. Then, boundedness and non-negativity of the solutions are discussed in detail. We then proceed to investigate the dynamics through the determination of three equilibrium points: disease-free equilibrium, human-endemic equilibrium, and endemic equilibrium. Local stability of these equilibrium points is analyzed with Jacobian matrices, while the global stability is established with Lyapunov functions, representing an additional theoretical contribution of this paper. Numerical simulations are conducted to illustrate and validate the analytical results.

The remainder of this paper is organized as follows. Section 2 is devoted to the formulation of the mathematical model describing Mpox transmission dynamics between humans and rodents. Section 3 is dedicated to the basic properties of well-posedness, boundedness, and non-negativity of solutions. In Section 4, we calculate the equilibrium points and the basic reproduction number characterizing the disease-free, human-endemic, and endemic states. Section 5 interprets the local and global stability of such equilibria, enabling us to determine the long-term behavior of the system. In Section 6, we carry out the sensitivity analysis that identifies the most sensitive parameters affecting the basic reproduction number. In Section 7, we present numerical simulations that support the analytical findings. Finally, in Section 8 we address the main conclusion and possible directions for further research.

2. MODEL FORMULATION

The transmission dynamics of Mpox are described in this developed mathematical model that contains human and rodent populations. For humans, there are five epidemiological compartments: susceptible individuals (S_h), vaccinated individuals (V_h), asymptomatic individuals (A_h), symptomatic infected individuals (I_h), and recovered individuals (R_h). Rodents are divided into two compartments: susceptible rodents (S_r) and infected rodents (I_r). The total human population at any given time is represented by the sum of all human subpopulations $N_h = S_h + V_h + A_h + I_h + R_h$. Similarly, the total rodent population is given by $N_r = S_r + I_r$. In general, interactions among subpopulations are influenced by various factors, necessitating several simplifying assumptions. In this mathematical model, it is assumed that all humans and rodents are born susceptible, vaccinated individuals do not experience waning immunity, recovered individuals are not subject to reinfection, and infected rodents do not recover.

In the human population, susceptible individuals increase at a constant recruitment rate (π_h) and may transition into vaccinated individuals at rate α_h, become infected through contact with infectious humans or rodents, or die naturally at rate μ_h. The human force of infection, $\lambda_h = \frac{\beta_1 A_h + \beta_2 I_h + \beta_3 I_r}{N_h}$, determines transmission dynamics in humans, where β_1, β_2, and β_3 represent the effective contact rates. Vaccinated individuals may recover at rate τ_1 or die naturally, while asymptomatic individuals, although not exhibiting symptoms, can transmit the virus, progress to symptomatic infection at rate γ_h, or die due to Mpox (δ_1) or natural causes. Symptomatic individuals recover at rate τ_2 or die due to disease (δ_2) or naturally. In the rodent population, susceptible rodents are recruited at rate π_r and become infected via contact with infected rodents at rate $\lambda_r = \frac{\beta_4 I_r}{N_r}$, where β_4 is the contact rate, while susceptible and infected rodents die due to natural mortality (μ_r) or Mpox-induced death (δ_3).

The transmission diagram of Mpox dynamics is illustrated in Figure 1. The description and corresponding values of each parameter in weeks are provided in Table 1.

Table 1: Description of parameters.

Parameter	Description	Value	Reference
π_h	Recruitment rate of susceptible humans	17500	[2], [26]
π_r	Recruitment rate of susceptible rodents	3.5	[2], [26]
α_h	Vaccination rate of susceptible humans	0.2104	[23]
β_1	Contact rate between susceptible and asymptomatic humans	0.19	[23]
β_2	Contact rate between susceptible and symptomatic humans	0.4192	[23]
β_3	Contact rate between susceptible humans and infected rodents	0.3632	[23]
β_4	Rodent-to-rodent contact rate	0.0257	[23]
γ_h	Progression rate to symptomatic infection	0.05	Assumed
τ_1	Effectiveness rate of vaccination	0.83	Assumed
τ_2	Recovery rate of symptomatic humans	0.3432	[23]
δ_1	Death rate of asymptomatic humans due to Mpox	0.00041	[23]
δ_2	Death rate of symptomatic humans due to Mpox	0.0012	[23]
δ_3	Death rate of infected rodents due to Mpox	0.00028	[23]
μ_h	Natural death rate of humans	0.00032	[2], [26]
μ_r	Natural death rate of rodents	0.014	[2], [26]

As illustrated in Figure 1, the transmission dynamics of Mpox are formulated through the following system of differential equations.

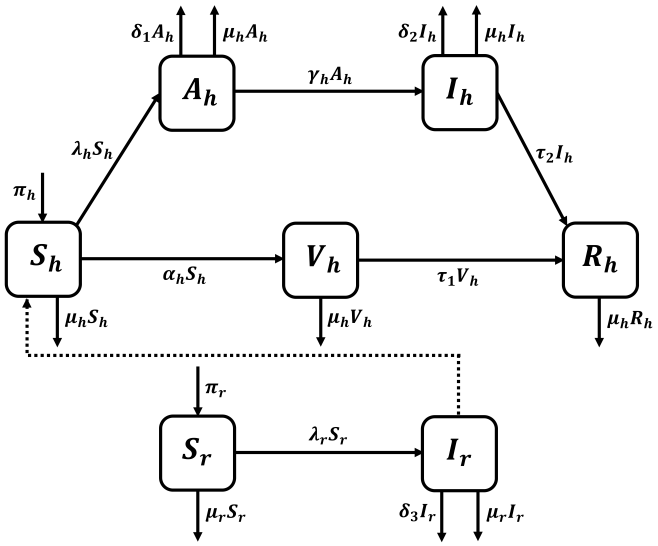

Figure 1: Transmission diagram of Mpox dynamics.

$$\begin{aligned}
\frac{dS_h}{dt} &= \pi_h - (\lambda_h + \alpha_h + \mu_h)S_h,\\
\frac{dV_h}{dt} &= \alpha_h S_h - (\tau_1 + \mu_h)V_h,\\
\frac{dA_h}{dt} &= \lambda_h S_h - (\gamma_h + \delta_1 + \mu_h)A_h,\\
\frac{dI_h}{dt} &= \gamma_h A_h - (\tau_2 + \delta_2 + \mu_h)I_h,\\
\frac{dR_h}{dt} &= \tau_1 V_h + \tau_2 I_h - \mu_h R_h,\\
\frac{dS_r}{dt} &= \pi_r - (\lambda_r + \mu_r)S_r,\\
\frac{dI_r}{dt} &= \lambda_r S_r - (\delta_3 + \mu_r)I_r,
\end{aligned} \tag{1}$$

with the initial conditions $S_h(0) > 0$, $V_h(0) \geq 0$, $A_h(0) \geq 0$, $I_h(0) \geq 0$, $R_h(0) \geq 0$, $S_r(0) > 0$, $I_r(0) \geq 0$.

3. Basic Properties of Model

3.1. Well-Posedness

A dynamical system is said to be well-posed if it satisfies three fundamental properties: existence, uniqueness, and stability of the solution [36]. In this section, we examine the well-posedness of system (1) by applying the contraction mapping principle, following the approach adopted by Elsonbaty et al. [19]. Consider the first differential equation of system (1):

$$\frac{dS_h}{dt} = \pi_h - (\lambda_h + \alpha_h + \mu_h)S_h.$$

By performing a simple integration, the integral form of the solution is expressed as

$$S_h(t) = S_h(0) + \int_0^t (\pi_h - (\lambda_h + \alpha_h + \mu_h)S_h)\, ds. \tag{2}$$

We define the operator P as follows

$$P(S_h(t)) = S_h(0) + \int_0^t (\pi_h - (\lambda_h + \alpha_h + \mu_h)S_h)\, ds. \tag{3}$$

Let X be a complete metric space defined by $X = \{S_h : [0,a] \to \mathbb{R} \mid S_h \text{ is continuous}\}$, with the metric

$$d(S_{h1}, S_{h2}) = \|S_{h1} - S_{h2}\|_\infty = \sup_{t\in[0,a]} |S_{h1}(t) - S_{h2}(t)|. \tag{4}$$

For any $S_{h_1}, S_{h_2} \in X$, we compute

$$\begin{aligned}
\left|P(S_{h_1}(t)) - P(S_{h_2}(t))\right| &= \left|\int_0^t -(\lambda_h + \alpha_h + \mu_h)\left(S_{h_1} - S_{h_2}\right) ds\right|, \\
&\leq \int_0^t \left|\lambda_h + \alpha_h + \mu_h\right| \left|S_{h_1} - S_{h_2}\right| ds, \\
&\leq K \int_0^t \left|S_{h_1} - S_{h_2}\right| ds, \\
&\leq Kt \left\|S_{h_1} - S_{h_2}\right\|_\infty,
\end{aligned}$$

where $K = \sup_{s\in[0,a]} (\lambda_h + \alpha_h + \mu_h)$.
Thus,

$$\|P(S_{h1}) - P(S_{h2})\|_\infty \leq Ka\|S_{h1} - S_{h2}\|_\infty. \tag{5}$$

To ensure that P is a contraction, the condition $Ka < 1$ must hold, which implies $a < \frac{1}{K}$. Therefore, over the interval $[0,a]$ where $a < \frac{1}{K}$, the operator P is a contraction on the space X. By the contraction mapping principle, there exists a unique $S_h(t) \in X$ such that $S_h(t) = P(S_h(t))$.

Next, we analyze the stability of the solution $S_h(t) \in X$. Let $S_{h1}(t)$ and $S_{h2}(t)$ be two solutions with different initial values $S_{h1}(0)$ and $S_{h2}(0)$, where $S_{h1}(0) \neq S_{h2}(0)$, satisfying

$$\begin{aligned}
S_{h1}(t) &= S_{h1}(0) + \int_0^t (\pi_h - (\lambda_h + \alpha_h + \mu_h)S_{h1}(s))\, ds, \\
S_{h2}(t) &= S_{h2}(0) + \int_0^t (\pi_h - (\lambda_h + \alpha_h + \mu_h)S_{h2}(s))\, ds.
\end{aligned} \tag{6}$$

Then,

$$\begin{aligned}
|S_{h1}(t) - S_{h2}(t)| &= \left|(S_{h1}(0) - S_{h2}(0)) + \int_0^t -(\lambda_h + \alpha_h + \mu_h)(S_{h1} - S_{h2})\, ds\right|, \\
&\leq |S_{h1}(0) - S_{h2}(0)| + \left|\int_0^t -(\lambda_h + \alpha_h + \mu_h)(S_{h1} - S_{h2})\, ds\right|.
\end{aligned}$$

Consequently, we obtain

$$\begin{aligned}
\|S_{h_1}(t) - S_{h_2}(t)\|_\infty &\leq \|S_{h_1}(0) - S_{h_2}(0)\|_\infty + Ka\, \|S_{h_1} - S_{h_2}\|_\infty, \\
(1 - Ka)\, \|S_{h_1}(t) - S_{h_2}(t)\|_\infty &\leq \|S_{h_1}(0) - S_{h_2}(0)\|_\infty.
\end{aligned}$$

By assuming $0 < \|S_{h1}(0) - S_{h2}(0)\|_\infty \leq \theta$, we conclude

$$0 < \|S_{h1}(t) - S_{h2}(t)\|_\infty \leq \frac{\theta}{1 - Ka} = \varepsilon, \tag{7}$$

where $Ka < 1$ and $K = \sup_{s\in[0,a]}(\lambda_h + \alpha_h + \mu_h)$.
Therefore, the solution $S_h(t) \in X$ satisfies the stability condition.

Furthermore, using a similar approach, it can be shown that the remaining state variables, namely $V_h(t)$, $A_h(t)$, $I_h(t)$, $R_h(t)$, $S_r(t)$, and $I_r(t)$, also satisfy the conditions of existence, uniqueness, and stability of solutions. Therefore, system (1) is considered well-posed.

3.2. Boundedness and Non-negativity

In this section, we establish the boundedness and the non-negativity of the solutions for system (1). Focusing first on the boundedness, starting with the human population, we observe that

$$\frac{dN_h}{dt} = \frac{dS_h}{dt} + \frac{dV_h}{dt} + \frac{dA_h}{dt} + \frac{dI_h}{dt} + \frac{dR_h}{dt},$$

which simplifies to

$$\frac{dN_h}{dt} = \pi_h - \mu_h N_h - \delta_1 A_h - \delta_2 I_h \leq \pi_h - \mu_h N_h. \tag{8}$$

The solution of differential inequality (8) is given by

$$N_h(t) \leq \frac{\pi_h}{\mu_h} + \left(N_h(0) - \frac{\pi_h}{\mu_h}\right) e^{-\mu_h t}. \tag{9}$$

Therefore, as $t \to \infty$, we have

$$\lim_{t\to\infty} N_h(t) \leq \frac{\pi_h}{\mu_h}. \tag{10}$$

Similarly, for the rodent population, we have

$$\frac{dN_r}{dt} = \frac{dS_r}{dt} + \frac{dI_r}{dt} = \pi_r - \mu_r N_r - \delta_3 I_r \leq \pi_r - \mu_r N_r. \tag{11}$$

The solution of differential inequality (11) is

$$N_r(t) \leq \frac{\pi_r}{\mu_r} + \left(N_r(0) - \frac{\pi_r}{\mu_r}\right) e^{-\mu_r t}. \tag{12}$$

Hence, as $t \to \infty$, it follows that

$$\lim_{t\to\infty} N_r(t) \leq \frac{\pi_r}{\mu_r}. \tag{13}$$

Consequently, the total human and rodent populations are respectively bounded by $\frac{\pi_h}{\mu_h}$ and $\frac{\pi_r}{\mu_r}$. Therefore, system (1) admits bounded solutions within the following feasible region:

$$\Omega = \left\{(S_h, V_h, A_h, I_h, R_h, S_r, I_r) \in \mathbb{R}^7_+ \mid N_h \leq \frac{\pi_h}{\mu_h},\ N_r \leq \frac{\pi_r}{\mu_r}\right\}. \tag{14}$$

Next, we analyze the non-negativity of the solutions for system (1), as stated in the following theorem.

Theorem 3.1. *Let $S_h(t), V_h(t), A_h(t), I_h(t), R_h(t), S_r(t)$, and $I_r(t)$ be solutions for system (1). If the initial conditions are non-negative, then the solutions remain non-negative for any time $t \geq 0$.*

Proof: Consider the first differential equation of system (1):

$$\frac{dS_h}{dt} = \pi_h - (\lambda_h + \alpha_h + \mu_h) S_h.$$

Multiplying both sides by the integrating factor $e^{(\alpha_h+\mu_h)t + \int_0^t \lambda_h\, ds}$, we obtain

$$\frac{d}{dt}\left(e^{(\alpha_h+\mu_h)t + \int_0^t \lambda_h\, ds} S_h\right) = \pi_h e^{(\alpha_h+\mu_h)t + \int_0^t \lambda_h\, ds}. \tag{15}$$

The solution of differential equation (15) is given by

$$S_h(t) = \left(\int_0^t \pi_h e^{(\alpha_h+\mu_h)y + \int_0^y \lambda_h\, ds} dy + S_h(0)\right) e^{-(\alpha_h+\mu_h)t - \int_0^t \lambda_h\, ds} \geq 0. \tag{16}$$

Hence, $S_h(t)$ remains non-negative for any time $t \geq 0$. By applying a similar argument to the other state variables, it can be shown that $V_h(t), A_h(t), I_h(t), R_h(t), S_r(t), I_r(t)$ are also non-negative for any time $t \geq 0$.

4. Equilibrium and Basic Reproduction Number

In this section, we determine the equilibrium points of system (1), which are obtained by setting the time derivatives of all state variables to zero [12]:

$$\frac{dS_h}{dt} = \frac{dV_h}{dt} = \frac{dA_h}{dt} = \frac{dI_h}{dt} = \frac{dR_h}{dt} = \frac{dS_r}{dt} = \frac{dI_r}{dt} = 0.$$

Consequently, system (1) reduces to the following set of algebraic equations:

$$\begin{aligned} \pi_h - (\lambda_h + k_1)S_h &= 0, \\ \alpha_h S_h - k_2 V_h &= 0, \\ \lambda_h S_h - k_3 A_h &= 0, \\ \gamma_h A_h - k_4 I_h &= 0, \\ \tau_1 V_h + \tau_2 I_h - \mu_h R_h &= 0, \\ \pi_r - (\lambda_r + \mu_r)S_r &= 0, \\ \lambda_r S_r - k_5 I_r &= 0, \end{aligned} \tag{17}$$

where

$$k_1 = \alpha_h + \mu_h, k_2 = \tau_1 + \mu_h, k_3 = \gamma_h + \delta_1 + \mu_h, k_4 = \tau_2 + \delta_2 + \mu_h, \text{ and } k_5 = \delta_3 + \mu_r. \tag{18}$$

The disease-free equilibrium (DFE) corresponds to the state in which no Mpox infection exists in the population, i.e., $A_h = I_h = I_r = 0$. The DFE for system (1) is given by

$$X^0 = (S_h^0, V_h^0, A_h^0, I_h^0, R_h^0, S_r^0, I_r^0),$$

with components

$$X^0 = \left(\frac{\pi_h}{k_1}, \frac{\alpha_h \pi_h}{k_1 k_2}, 0, 0, \frac{\alpha_h \pi_h \tau_1}{k_1 k_2 \mu_h}, \frac{\pi_r}{\mu_r}, 0\right). \tag{19}$$

Next, we derive the basic reproduction number $\mathcal{R}_0$, which is defined as the expected number of secondary infections generated by a single infected individual in a fully susceptible population [24]. In this research, $\mathcal{R}_0$ is computed using the next-generation matrix (NGM) method [18]. The infected compartments in system (1) are A_h, I_h, and I_r, and the dynamics of the infected subsystem are represented as

$$\begin{pmatrix} \frac{dA_h}{dt} \\ \frac{dI_h}{dt} \\ \frac{dI_r}{dt} \end{pmatrix} = \begin{pmatrix} \lambda_h S_h \\ 0 \\ \lambda_r S_r \end{pmatrix} - \begin{pmatrix} k_3 A_h \\ -\gamma_h A_h + k_4 I_h \\ k_5 I_r \end{pmatrix}. \tag{20}$$

Linearizing system (20) leads to the construction of matrices F and V:

$$F = \begin{pmatrix} \frac{(\beta_1 - \lambda_h)S_h}{N_h} & \frac{(\beta_2 - \lambda_h)S_h}{N_h} & \frac{\beta_3 S_h}{N_h} \\ 0 & 0 & 0 \\ 0 & 0 & \frac{(\beta_4 - \lambda_r)S_r}{N_r} \end{pmatrix}, \quad V = \begin{pmatrix} k_3 & 0 & 0 \\ -\gamma_h & k_4 & 0 \\ 0 & 0 & k_5 \end{pmatrix}. \tag{21}$$

Substituting DFE (19) into F and V, we obtain

$$\mathbb{F} = \begin{pmatrix} \frac{\beta_1 \mu_h}{k_1} & \frac{\beta_2 \mu_h}{k_1} & \frac{\beta_3 \mu_h}{k_1} \\ 0 & 0 & 0 \\ 0 & 0 & \beta_4 \end{pmatrix}, \quad \mathbb{V} = \begin{pmatrix} k_3 & 0 & 0 \\ -\gamma_h & k_4 & 0 \\ 0 & 0 & k_5 \end{pmatrix}. \tag{22}$$

The next-generation matrix $K = \mathbb{F}\mathbb{V}^{-1}$ is then calculated as

$$K = \begin{pmatrix} \frac{\beta_1 \mu_h k_4 + \beta_2 \mu_h \gamma_h}{k_1 k_3 k_4} & \frac{\beta_2 \mu_h}{k_1 k_4} & \frac{\beta_3 \mu_h}{k_1 k_5} \\ 0 & 0 & 0 \\ 0 & 0 & \frac{\beta_4}{k_5} \end{pmatrix}. \tag{23}$$

The eigenvalues of K are

$$\lambda_1 = 0,\ \lambda_2 = \frac{\beta_1\mu_h k_4 + \beta_2\mu_h\gamma_h}{k_1k_3k_4},\ \text{and}\ \lambda_3 = \frac{\beta_4}{k_5}.$$

Thus, the basic reproduction number is given by

$$\mathcal{R}_0 = \max\left\{\mathcal{R}_0^h, \mathcal{R}_0^r\right\} = \max\left\{\frac{\beta_1\mu_h k_4 + \beta_2\mu_h\gamma_h}{k_1k_3k_4}, \frac{\beta_4}{k_5}\right\}. \tag{24}$$

The next step, we determine the endemic equilibrium of system (1), which corresponds to the state in which Mpox persists in the population. There are two types of endemic equilibria in system (1): human-endemic equilibrium (HEE) and endemic equilibrium (EE). The HEE arises when Mpox infection is present in the human population but not in rodents, i.e., $A_h \neq 0$, $I_h \neq 0$, but $I_r = 0$. Under this condition, the HEE is expressed as

$$X^+ = (S_h^+, V_h^+, A_h^+, I_h^+, R_h^+, S_r^+, I_r^+), \tag{25}$$

where

$$S_h^+ = \frac{\pi_h}{\lambda_h^+ + k_1},\quad V_h^+ = \frac{\alpha_h\pi_h}{(\lambda_h^+ + k_1)k_2},\quad A_h^+ = \frac{\pi_h\lambda_h^+}{(\lambda_h^+ + k_1)k_3},\quad I_h^+ = \frac{\pi_h\gamma_h\lambda_h^+}{(\lambda_h^+ + k_1)k_3k_4},$$
$$R_h^+ = \frac{\alpha_h\pi_h\tau_1k_3k_4 + \pi_h\tau_2\gamma_h\lambda_h^+k_2}{(\lambda_h^+ + k_1)k_2k_3k_4\mu_h},\quad S_r^+ = \frac{\pi_r}{\mu_r},\quad I_r^+ = 0,$$

and the infection rate λ_h^+ is given by

$$\lambda_h^+ = \frac{k_1k_3k_4(\mathcal{R}_0^h - 1)}{k_4\mu_h + \tau_2\gamma_h + \gamma_h\mu_h}. \tag{26}$$

It follows that the HEE exists if and only if $\mathcal{R}_0^h > 1$.

The endemic equilibrium (EE) refers to the condition in which both human and rodent populations are actively infected by Mpox, i.e., $A_h \neq 0$, $I_h \neq 0$, and $I_r \neq 0$. In this case, the EE is represented as

$$X^* = (S_h^*, V_h^*, A_h^*, I_h^*, R_h^*, S_r^*, I_r^*), \tag{27}$$

where

$$S_h^* = \frac{\pi_h}{\lambda_h^* + k_1},\quad V_h^* = \frac{\alpha_h\pi_h}{(\lambda_h^* + k_1)k_2},\quad A_h^* = \frac{\pi_h\lambda_h^*}{(\lambda_h^* + k_1)k_3},\quad I_h^* = \frac{\pi_h\gamma_h\lambda_h^*}{(\lambda_h^* + k_1)k_3k_4},$$
$$R_h^* = \frac{\alpha_h\pi_h\tau_1k_3k_4 + \pi_h\tau_2\gamma_h\lambda_h^*k_2}{(\lambda_h^* + k_1)k_2k_3k_4\mu_h},\quad S_r^* = \frac{\pi_r}{\lambda_r^* + \mu_r},\quad I_r^* = \frac{\pi_r\lambda_r^*}{k_5(\lambda_r^* + \mu_r)},$$

with

$$\lambda_r^* = k_5(\mathcal{R}_0^r - 1), \tag{28}$$

and the infection rate λ_h^* is the positive root of the quadratic equation

$$a{\lambda_h^*}^2 + b\lambda_h^* + c = 0, \tag{29}$$

where the coefficients are defined as

$a = \pi_h k_5(\lambda_r^* + \mu_r)(k_4\mu_h + \tau_2\gamma_h + \gamma_h\mu_h),$
$b = \pi_h k_1k_3k_4k_5(\lambda_r^* + \mu_r)(1 - \mathcal{R}_0^h) - \beta_3\pi_r\lambda_r^*k_3k_4,$
$c = -\beta_3\pi_r\mu_h\lambda_r^*k_1k_3k_4.$

From the analytical expression, when $\mathcal{R}_0^r = 1$, this means $X^* = X^+$. Hence, for the endemic state to occur, it is necessary that $\lambda_r^* > 0$, which happens when $\mathcal{R}_0^r > 1$. Since all parameters are positive, we have $a > 0$ and $c < 0$, ensuring that a unique positive solution for λ_h^* exists. Specifically, for the condition $\mathcal{R}_0^h \geq 1$, then $b < 0$, which gives $\lambda_h^* = \frac{-b+\sqrt{b^2-4ac}}{2a} > 0$. Therefore, the EE exists and is unique if and only if $\mathcal{R}_0^r > 1$.

Based on the previous analysis, the existence criteria of the equilibrium points can be summarized as follows: the disease-free equilibrium (DFE) always exists, the human-endemic equilibrium (HEE) exists when $\mathcal{R}_0^h > 1$, and the endemic equilibrium (EE) exists when $\mathcal{R}_0^r > 1$. These criteria are illustrated as existence regions in Figure 2.

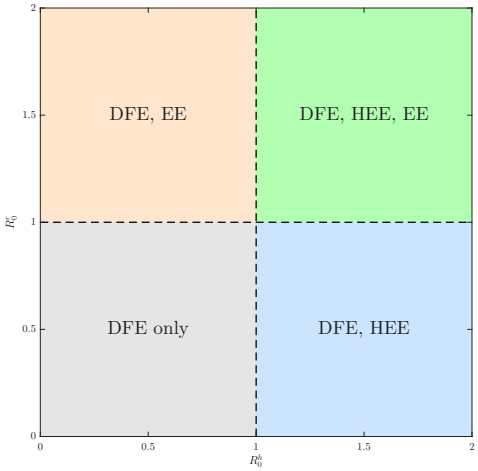

Figure 2: Existence regions of equilibrium points based on $\mathcal{R}_0^h$ and $\mathcal{R}_0^r$.

5. Stability of Equilibrium

5.1. Stability of Disease-Free Equilibrium

In this section, we analyze both the local and global stability of the disease-free equilibrium (DFE) of system (1). The local stability is examined through linearization using the Jacobian matrix, as stated in the following theorem.

Theorem 5.1. *The DFE of system (1) is locally asymptotically stable if and only if* $\mathcal{R}_0 < 1$.

Proof: The Jacobian matrix of system (1) is given by

$$J = \begin{pmatrix} A-\lambda_h-k_1 & A & B_1 & B_2 & A & A & C \\ \alpha_h & -k_2 & 0 & 0 & 0 & 0 & 0 \\ -A+\lambda_h & -A & -B_1-k_3 & -B_2 & -A & -A & -C \\ 0 & 0 & \gamma_h & -k_4 & 0 & 0 & 0 \\ 0 & \tau_1 & 0 & \tau_2 & -\mu_h & 0 & 0 \\ 0 & 0 & 0 & 0 & 0 & D-\lambda_r-\mu_r & E \\ 0 & 0 & 0 & 0 & 0 & -D+\lambda_r & -E-k_5 \end{pmatrix}, \tag{30}$$

where $A = \frac{\lambda_h S_h}{N_h}, B_i = \frac{(\lambda_h-\beta_i)S_h}{N_h}, C = \frac{-\beta_3 S_h}{N_h}, D = \frac{\lambda_r S_r}{N_r}, E = \frac{(\lambda_r-\beta_4)S_r}{N_r}$, and the terms k_1 to k_5 are defined in (18).
Substituting the DFE (19) into Jacobian matrix (30) yields

$$J(X^0) = \begin{pmatrix} -k_1 & 0 & -a_1 & -a_2 & 0 & 0 & -a_3 \\ \alpha_h & -k_2 & 0 & 0 & 0 & 0 & 0 \\ 0 & 0 & a_1-k_3 & a_2 & 0 & 0 & a_3 \\ 0 & 0 & \gamma_h & -k_4 & 0 & 0 & 0 \\ 0 & \tau_1 & 0 & \tau_2 & -\mu_h & 0 & 0 \\ 0 & 0 & 0 & 0 & 0 & -\mu_r & -\beta_4 \\ 0 & 0 & 0 & 0 & 0 & 0 & \beta_4-k_5 \end{pmatrix}, \tag{31}$$

where $a_j = \dfrac{\beta_j \mu_h}{k_1}$.
The characteristic equation derived from matrix (31) is

$$(k_1+\lambda)(k_2+\lambda)(\mu_h+\lambda)(\mu_r+\lambda)(-\beta_4+k_5+\lambda)(\lambda^2+m_1\lambda+m_2)=0, \tag{32}$$

where

$$m_1 = \frac{k_1k_3k_4(1-\mathcal{R}_0^h)+\beta_2\mu_h\gamma_h+k_1k_4^2}{k_1k_4} \text{ and } m_2 = \frac{k_1k_3k_4(1-\mathcal{R}_0^h)}{k_1}.$$

The eigenvalues are $\lambda_1=-k_1, \lambda_2=-k_2, \lambda_3=-\mu_h, \lambda_4=-\mu_r, \lambda_5=\beta_4-k_5$, and the roots of the quadratic equation

$$\lambda^2+m_1\lambda+m_2=0. \tag{33}$$

It is evident that $\lambda_1, \lambda_2, \lambda_3, \lambda_4 < 0$, and $\lambda_5 < 0$ if and only if $\mathcal{R}_0^r < 1$, since $\lambda_5 = \beta_4 - k_5 = k_5(\mathcal{R}_0^r - 1) < 0$. According to the Routh-Hurwitz criterion [11], the roots of the quadratic equation (33) will have negative real parts if and only if $m_1 > 0$ and $m_2 > 0$, which holds true when $\mathcal{R}_0^h < 1$. Therefore, the DFE of system (1) is locally asymptotically stable if and only if $\mathcal{R}_0 < 1$.

Next, to establish global stability, we apply a Lyapunov function [32] as stated in the following theorem.

Theorem 5.2. *The DFE of system (1) is globally asymptotically stable if and only if* $\mathcal{R}_0 < 1$.

Proof: Consider the Lyapunov function $L : D \to \mathbb{R}$ defined as

$$L = C_1A_h + C_2I_h + C_3I_r, \tag{34}$$

where $C_1, C_2, C_3 > 0$.
It can be observed that $L(X^0) = C_1A_h^0 + C_2I_h^0 + C_3I_r^0 = 0$, and for any state different from the DFE, we have $L > 0$. Next, taking the time derivative of L, we obtain

$$\frac{\partial L}{\partial t} \le \left(\frac{C_1(\beta_1\mu_h - k_1k_3)}{k_1} + C_2\gamma_h\right)A_h + \left(\frac{C_1\beta_2\mu_h}{k_1} - C_2k_4\right)I_h + \left(\frac{C_1\beta_3\mu_h}{k_1} + C_3(\beta_4-k_5)\right)I_r. \tag{35}$$

To eliminate the coefficient of A_h, set

$$C_1 = \frac{-\gamma_h k_1}{\beta_1\mu_h - k_1k_3}, \quad C_2 = 1. \tag{36}$$

Since $C_1 > 0$ and $\gamma_h k_1 > 0$, it follows that $\beta_1\mu_h - k_1k_3 < 0$.
Choose $C_3 > 0$ as

$$C_3 = \frac{\beta_3k_4}{\beta_2k_5(1-\mathcal{R}_0^r)}, \tag{37}$$

where $\mathcal{R}_0^r < 1$.
Substituting C_1, C_2, and C_3 into differential inequality (35), we get

$$\frac{\partial L}{\partial t} \le \frac{k_1k_3k_4(1-\mathcal{R}_0^h)}{\beta_1\mu_h - k_1k_3}I_h + \frac{\beta_3k_1k_3k_4(1-\mathcal{R}_0^h)}{(\beta_1\mu_h - k_1k_3)\beta_2}I_r. \tag{38}$$

Consequently, for both coefficients of I_h and I_r to be negative, it is required that $\mathcal{R}_0^h < 1$. Thus, the time derivative of Lyapunov function L satisfies $\frac{\partial L}{\partial t} < 0$ if and only if $\mathcal{R}_0 < 1$, and $\frac{\partial L}{\partial t} = 0$ holds only when $A_h = A_h^0$, $I_h = I_h^0$, and $I_r = I_r^0$. By LaSalle's invariance principle [22], this ensures that all trajectories converge to the DFE. Therefore, the DFE of system (1) is globally asymptotically stable if and only if $\mathcal{R}_0 < 1$.

5.2. Global Stability of Endemic Equilibrium

In this section, we investigate the global stability of the human-endemic equilibrium (HEE) and the endemic equilibrium (EE) of system (1) by constructing Lyapunov functions [32]. The global stability of the human-endemic equilibrium (HEE) is presented in the following theorem.

Theorem 5.3. *Let $\mathcal{R}_0^h > 1$ such that the HEE exists. The HEE of system (1) is globally asymptotically stable if and only if $\mathcal{R}_0^r < 1$.*

Proof: Define a Lyapunov function $L : D \to \mathbb{R}$ as follows

$$L = \left(S_h - S_h^+ - S_h^+ \ln \frac{S_h}{S_h^+}\right) + p_1 \left(V_h - V_h^+ - V_h^+ \ln \frac{V_h}{V_h^+}\right) + \left(A_h - A_h^+ - A_h^+ \ln \frac{A_h}{A_h^+}\right) + p_2 \left(I_h - I_h^+ - I_h^+ \ln \frac{I_h}{I_h^+}\right) + p_3 \left(S_r - S_r^+ - S_r^+ \ln \frac{S_r}{S_r^+}\right) + p_4 I_r. \tag{39}$$

where $p_1 = \frac{\beta_1 A_h^+}{\alpha_h N_h^+}$, $p_2 = \frac{\beta_2 I_h^+ S_h^+}{\gamma_h A_h^+ N_h^+}$, $p_3 = \frac{S_r^+}{\beta_4}$, and $p_4 = \frac{S_r^+}{k_5(1-\mathcal{R}_0^r)}$ with $\mathcal{R}_0^r < 1$.
Let $L_1 = S_h - S_h^+ - S_h^+ \ln \frac{S_h}{S_h^+}$, and similarly define L_2 through L_5. It can be seen that $L(X^+) = L_1^+ + p_1 L_2^+ + L_3^+ + p_2 L_4^+ + p_3 L_5^+ + p_4 I_r^+ = 0$. Next, let $y = \frac{S_h}{S_h^+}$, and define $f(y) = y - 1 - \ln y$. Then $f'(y) = 1 - \frac{1}{y}$, which implies $f(y)$ is decreasing for $0 < y < 1$ and increasing for $y > 1$, achieving a global minimum at $y = 1$ with $f(1) = 0$. Thus, when $S_h \neq S_h^+$, it follows that $L_1 > 0$. By the same argument, $L_2, L_3, L_4, L_5 > 0$, hence $L > 0$. Next, taking the time derivative of L gives

$$\frac{\partial L}{\partial t} = \left(1 - \frac{S_h^+}{S_h}\right) \frac{dS_h}{dt} + p_1 \left(1 - \frac{V_h^+}{V_h}\right) \frac{dV_h}{dt} + \left(1 - \frac{A_h^+}{A_h}\right) \frac{dA_h}{dt} + p_2 \left(1 - \frac{I_h^+}{I_h}\right) \frac{dI_h}{dt} + p_3 \left(1 - \frac{S_r^+}{S_r}\right) \frac{dS_r}{dt} + p_4 \frac{dI_r}{dt}. \tag{40}$$

Substituting system (1) into differential equation (40), we have

$$\frac{\partial L}{\partial t} = \left(1 - \frac{S_h^+}{S_h}\right) (\pi_h - (\lambda_h + k_1) S_h) + p_1 \left(1 - \frac{V_h^+}{V_h}\right) (\alpha_h S_h - k_2 V_h) + \left(1 - \frac{A_h^+}{A_h}\right) (\lambda_h S_h - k_3 A_h) + p_2 \left(1 - \frac{I_h^+}{I_h}\right) (\gamma_h A_h - k_4 I_h) + p_3 \left(1 - \frac{S_r^+}{S_r}\right) (\pi_r - (\lambda_r + \mu_r) S_r) + p_4 (\lambda_r S_r - k_5 I_r).$$

At HEE, the following relationships are derived from system (17):

$$\pi_h = (\lambda_h^+ + k_1) S_h^+, \quad k_2 = \frac{\alpha_h S_h^+}{V_h^+}, \quad k_3 = \frac{\lambda_h^+ S_h^+}{A_h^+}, \quad k_4 = \frac{\gamma_h A_h^+}{I_h^+}, \quad \pi_r = (\lambda_r^+ + \mu_r) S_r^+.$$

By inserting these relationships into the preceding equation and applying algebraic manipulation with the substitutions p_1, p_2, p_3, p_4, λ_h, λ_h^+, λ_r, λ_r^+ and under the assumptions that $S_r \leq S_r^+$, $N_h = N_h^+$, $N_r = N_r^+$, $\frac{S_h^+}{S_h} + \frac{A_h}{A_h^+} \leq 2$, we get

$$\frac{\partial L}{\partial t} \leq k_1 S_h^+ \left(2 - \frac{S_h}{S_h^+} - \frac{S_h^+}{S_h}\right) + \frac{\beta_1 A_h^+ S_h^+}{N_h^+} \left(3 - \frac{S_h^+}{S_h} - \frac{V_h}{V_h^+} - \frac{S_h V_h^+}{S_h^+ V_h}\right) + \frac{\beta_2 I_h^+ S_h^+}{N_h^+} \left(3 - \frac{S_h^+}{S_h} - \frac{A_h I_h^+}{A_h^+ I_h} - \frac{I_h S_h A_h^+}{I_h^+ S_h^+ A_h}\right) + \frac{\beta_3 I_r S_h^+}{N_h^+} \left(3 - \frac{S_h^+}{S_h} - \frac{A_h}{A_h^+} - \frac{S_h A_h^+}{S_h^+ A_h}\right) + \frac{\mu_r {S_r^+}^2}{\beta_4} \left(2 - \frac{S_r}{S_r^+} - \frac{S_r^+}{S_r}\right) - S_r I_r. \tag{41}$$

Using the arithmetic-geometric mean inequality, we have

$$\left(2-\frac{S_h}{S_h^+}-\frac{S_h^+}{S_h}\right)\leq 0,\left(3-\frac{S_h^+}{S_h}-\frac{V_h}{V_h^+}-\frac{S_hV_h^+}{S_h^+V_h}\right)\leq 0,\left(3-\frac{S_h^+}{S_h}-\frac{A_hI_h^+}{A_h^+I_h}-\frac{I_hS_hA_h^+}{I_h^+S_h^+A_h}\right)\leq 0,$$
$$\left(3-\frac{S_h^+}{S_h}-\frac{A_h}{A_h^+}-\frac{S_hA_h^+}{S_h^+A_h}\right)\leq 0,\left(2-\frac{S_r}{S_r^+}-\frac{S_r^+}{S_r}\right)\leq 0.$$

Thus, the time derivative of Lyapunov function L satisfies $\frac{\partial L}{\partial t}<0$ if and only if $\mathcal{R}_0^r<1$. Moreover, $\frac{\partial L}{\partial t}=0$ only when $S_h=S_h^+$, $V_h=V_h^+$, $A_h=A_h^+$, $I_h=I_h^+$, $S_r=S_r^+$, and $I_r=I_r^+$. According to LaSalle's invariance principle [22], this implies that all trajectories converge to the HEE. Therefore, the HEE of system (1) is globally asymptotically stable if and only if $\mathcal{R}_0^r<1$.

Next, we examine the global stability of the endemic equilibrium (EE) of system (1), as presented in the following theorem.

Theorem 5.4. *Let $\mathcal{R}_0^r>1$ such that the EE exists. The EE of system (1) is globally asymptotically stable.*

Proof: Define a Lyapunov function $L\colon D\to\mathbb{R}$ as follows

$$\begin{aligned}L=&\left(S_h-S_h^*-S_h^*\ln\frac{S_h}{S_h^*}\right)+q_1\left(V_h-V_h^*-V_h^*\ln\frac{V_h}{V_h^*}\right)+\left(A_h-A_h^*-A_h^*\ln\frac{A_h}{A_h^*}\right)+\\&q_2\left(I_h-I_h^*-I_h^*\ln\frac{I_h}{I_h^*}\right)+\left(S_r-S_r^*-S_r^*\ln\frac{S_r}{S_r^*}\right)+\left(I_r-I_r^*-I_r^*\ln\frac{I_r}{I_r^*}\right),\end{aligned}\tag{42}$$

where $q_1=\frac{\beta_1A_h^*}{\alpha_hN_h^*}$ and $q_2=\frac{\beta_2I_h^*S_h^*}{\gamma_hA_h^*N_h^*}$.
It is clear that $L(X^*)=L_1^*+q_1L_2^*+L_3^*+q_2L_4^*+L_5^*+L_6^*=0$. By analyzing the convexity properties of each component, it follows that $L>0$ for all state variables not equal to the EE. Next, taking the time derivative of L yields

$$\begin{aligned}\frac{\partial L}{\partial t}=&\left(1-\frac{S_h^*}{S_h}\right)\frac{dS_h}{dt}+q_1\left(1-\frac{V_h^*}{V_h}\right)\frac{dV_h}{dt}+\left(1-\frac{A_h^*}{A_h}\right)\frac{dA_h}{dt}+q_2\left(1-\frac{I_h^*}{I_h}\right)\frac{dI_h}{dt}+\\&\left(1-\frac{S_r^*}{S_r}\right)\frac{dS_r}{dt}+\left(1-\frac{I_r^*}{I_r}\right)\frac{dI_r}{dt}.\end{aligned}\tag{43}$$

By following the same approach used in the proof of Theorem 5.3, and assuming that $N_h=N_h^*$, $N_r=N_r^*$, and $\frac{I_r}{I_r^*}+\frac{I_r^*}{I_r}\leq 2$, we have

$$\begin{aligned}\frac{\partial L}{\partial t}\leq&\, k_1S_h^*\left(2-\frac{S_h}{S_h^*}-\frac{S_h^*}{S_h}\right)+\frac{\beta_1A_h^*S_h^*}{N_h^*}\left(3-\frac{S_h^*}{S_h}-\frac{V_h}{V_h^*}-\frac{S_hV_h^*}{S_h^*V_h}\right)+\\&\frac{\beta_2I_h^*S_h^*}{N_h^*}\left(3-\frac{S_h^*}{S_h}-\frac{A_hI_h^*}{A_h^*I_h}-\frac{I_hS_hA_h^*}{I_h^*S_h^*A_h}\right)+\frac{\beta_3I_r^*S_h^*}{N_h^*}\left(4-\frac{S_h^*}{S_h}-\frac{I_r^*}{I_r}-\frac{A_h}{A_h^*}-\frac{I_rS_hA_h^*}{I_r^*S_h^*A_h}\right)\\&+\frac{\beta_4I_r^*S_r^*}{N_r^*}\left(2-\frac{S_r}{S_r^*}-\frac{S_r^*}{S_r}\right)+\mu_rS_r^*\left(2-\frac{S_r}{S_r^*}-\frac{S_r^*}{S_r}\right).\end{aligned}\tag{44}$$

Using the arithmetic-geometric mean inequality, we have

$$\left(2-\frac{S_h}{S_h^*}-\frac{S_h^*}{S_h}\right)\leq 0,\left(3-\frac{S_h^*}{S_h}-\frac{V_h}{V_h^*}-\frac{S_hV_h^*}{S_h^*V_h}\right)\leq 0,\left(3-\frac{S_h^*}{S_h}-\frac{A_hI_h^*}{A_h^*I_h}-\frac{I_hS_hA_h^*}{I_h^*S_h^*A_h}\right)\leq 0,$$
$$\left(4-\frac{S_h^*}{S_h}-\frac{I_r^*}{I_r}-\frac{A_h}{A_h^*}-\frac{I_rS_hA_h^*}{I_r^*S_h^*A_h}\right)\leq 0,\left(2-\frac{S_r}{S_r^*}-\frac{S_r^*}{S_r}\right)\leq 0.$$

Thus, the time derivative of the Lyapunov function L satisfies $\frac{\partial L}{\partial t}<0$, and $\frac{\partial L}{\partial t}=0$ if and only if $S_h=S_h^*$, $V_h=V_h^*$, $A_h=A_h^*$, $I_h=I_h^*$, $S_r=S_r^*$, and $I_r=I_r^*$. By LaSalle's invariance principle [22], this

guarantees that all trajectories converge to the EE. Therefore, the EE of system (1) is globally asymptotically stable.

Based on the stability analysis, the global stability criteria of the equilibrium points can be summarized as follows: the disease-free equilibrium (DFE) is globally asymptotically stable when $\mathcal{R}_0 = \max\{\mathcal{R}_0^h, \mathcal{R}_0^r\} < 1$, the human-endemic equilibrium (HEE) exists and is globally asymptotically stable when $\mathcal{R}_0^h > 1$ and $\mathcal{R}_0^r < 1$, and the endemic equilibrium (EE) exists and is globally asymptotically stable when $\mathcal{R}_0^r > 1$. These criteria are visualized as global asymptotic stability regions in Figure 3.

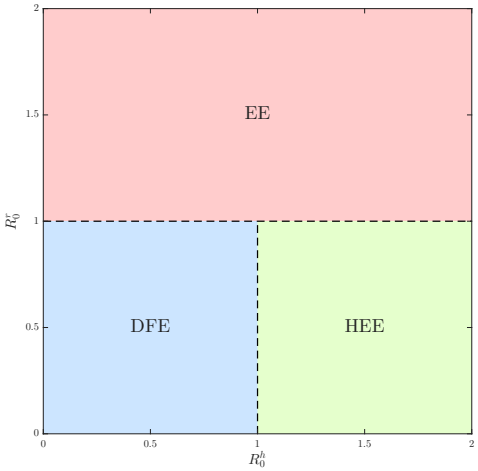

Figure 3: Global asymptotic stability regions of equilibrium points based on $\mathcal{R}_0^h$ and $\mathcal{R}_0^r$.

6. Sensitivity Analysis

In this section, we present a sensitivity analysis to identify the parameters that most significantly affect the stability conditions of the equilibrium points of system (1). The sensitivity index for each parameter is computed using the following expression.

$$e_x = \frac{x}{\mathcal{R}_0} \times \frac{\partial \mathcal{R}_0}{\partial x}, \tag{45}$$

where x, $\mathcal{R}_0$, and e_x denote the parameter of interest, the basic reproduction number, and the sensitivity index of x with respect to $\mathcal{R}_0$, respectively [16].

Table 2: Sensitivity indices.

Parameter	Sensitivity index w.r.t. $\mathcal{R}_0^h$	Sensitivity index w.r.t. $\mathcal{R}_0^r$
α_h	-0.99851	–
β_1	0.75756	–
β_2	0.24244	–
β_4	–	1
γ_h	-0.74327	–
τ_2	-0.24137	–
δ_1	-0.00808	–
δ_2	-0.00084	–
δ_3	–	-0.01961
μ_h	0.99195	–
μ_r	–	-0.98039

A positive sensitivity index means that with an increase or decrease in the corresponding parameter, there is a corresponding increase or decrease in $\mathcal{R}_0$. In contrast, a negative sensitivity index implies that an increase

or decrease in the parameter decreases or increases $\mathcal{R}_0$, respectively. Based on the values in Table 1, the computed sensitivity indices for each parameter included in $\mathcal{R}_0$ are summarized in Table 2. Based on the results, parameters β_1, β_2, and μ_h exhibit positive sensitivity indices with respect to $\mathcal{R}_0^h$, indicating that increases in these parameters will raise the value of $\mathcal{R}_0^h$. In contrast, parameters α_h, γ_h, τ_2, δ_1, and δ_2 have negative sensitivity indices with respect to $\mathcal{R}_0^h$, meaning that increases in these parameters will reduce $\mathcal{R}_0^h$. Regarding $\mathcal{R}_0^r$, only β_4 has a positive sensitivity index, whereas δ_3 and μ_r have negative indices.

Table 3: Impact of parameter variations with respect to $\mathcal{R}_0$.

Parameter (p)	**Sensitivity index**		$\mathcal{R}_0^h = 0.00739$		$\mathcal{R}_0^r = 1.79972$	
	w.r.t. $\mathcal{R}_0^h$	**w.r.t. $\mathcal{R}_0^r$**	$p-10\%$	$p+10\%$	$p-10\%$	$p+10\%$
α_h	-0.99851	–	0.00813	0.00665	–	–
β_1	0.75756	–	0.00683	0.00795	–	–
β_2	0.24244	–	0.00721	0.00757	–	–
β_4	–	1	–	–	1.61975	1.97969
γ_h	-0.74327	–	0.00794	0.00684	–	–
τ_2	-0.24137	–	0.00757	0.00721	–	–
δ_1	-0.00808	–	0.00740	0.00739	–	–
δ_2	-0.00084	–	0.00739	0.00739	–	–
δ_3	–	-0.01961	–	–	1.80325	1.79619
μ_h	0.99195	–	0.00666	0.00812	–	–
μ_r	–	-0.98039	–	–	1.97616	1.62328

Table 3 presents the impact of $\pm$ 10% changes in parameter values with respect to $\mathcal{R}_0^h$ and $\mathcal{R}_0^r$. Based on the results, the sensitivity index of parameter β_1 with respect to $\mathcal{R}_0^h$ is 0.75756, indicating that a 10% increase (or decrease) in the effective contact rate between susceptible and asymptomatic individuals results in a 7.5756% increase (or decrease) in $\mathcal{R}_0^h$. On the other hand, the sensitivity index of α_h is -0.99851, meaning that a 10% increase (or decrease) in the vaccination rate of susceptible individuals leads to a 9.9851% decrease (or increase) in $\mathcal{R}_0^h$. Similar analyses apply to other parameters including β_2, β_4, γ_h, τ_2, δ_1, δ_2, δ_3, μ_h, and μ_r. Overall, the most influential parameters on $\mathcal{R}_0^h$ are α_h and μ_h, as they have the highest absolute sensitivity indices. For $\mathcal{R}_0^r$, the parameters with the greatest influence are β_4 and μ_r. However, since the natural death rate of humans (μ_h) and rodents (μ_r) are generally not subject to intervention, the most impactful controllable parameters are β_1 and α_h in the human population, and parameters β_4 and δ_3 in the rodent population.

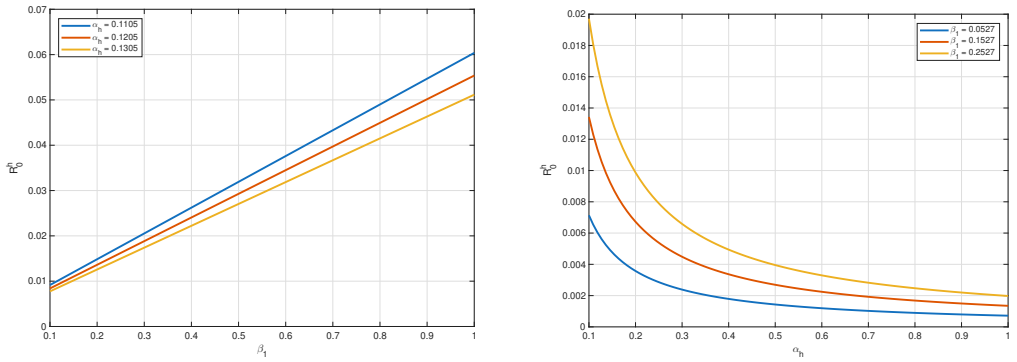

(a) (b)

Figure 4: Sensitivity of β_1 (panel (a)) and α_h (panel (b)) with respect to $\mathcal{R}_0^h$.

Next, we conduct the sensitivity simulations of parameters β_1 and α_h with respect to $\mathcal{R}_0^h$ in Figure 4. In panel (a), the values $\alpha_h = 0.1105$, $\alpha_h = 0.1205$, and $\alpha_h = 0.1305$ are selected, while β_1 varies within the

interval $0.1 \leq \beta_1 \leq 1$. This panel illustrates that an increase in parameter β_1 results in an increase in $\mathcal{R}_0^h$ for all values of α_h. In panel (b), the values $\beta_1 = 0.0527$, $\beta_1 = 0.1527$, and $\beta_1 = 0.2527$ are selected, while α_h varies within the interval $0.1 \leq \alpha_h \leq 1$. This panel illustrates that an increase in parameter α_h leads to a decrease in $\mathcal{R}_0^h$ for all values of β_1.

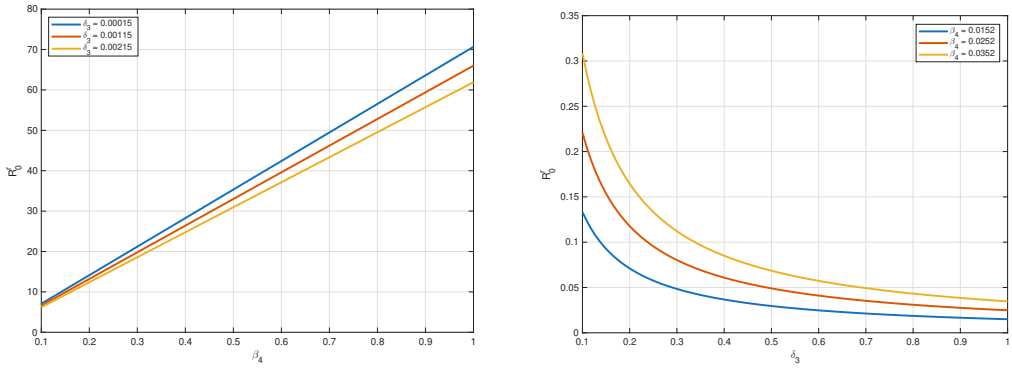

(a) (b)

Figure 5: Sensitivity of β_4 (panel (a)) and δ_3 (panel (b)) with respect to $\mathcal{R}_0^r$.

Figure 5 presents the sensitivity simulation of parameters β_4 and δ_3 with respect to $\mathcal{R}_0^r$. In panel (a), the values $\delta_3 = 0.00015$, $\delta_3 = 0.00115$, and $\delta_3 = 0.00215$ are selected, while β_4 varies within the interval $0.1 \leq \beta_4 \leq 1$. This panel illustrates that an increase in parameter β_4 results in an increase in $\mathcal{R}_0^r$ for all values of δ_3. For the sensitivity simulation of parameter δ_3 with respect to $\mathcal{R}_0^r$ in panel (b), the values $\beta_4 = 0.0152$, $\beta_4 = 0.0252$, and $\beta_4 = 0.0352$ are selected, while δ_3 varies within the interval $0.1 \leq \delta_3 \leq 1$. This panel illustrates that an increase in parameter δ_3 leads to a decrease in $\mathcal{R}_0^r$ for all values of β_4.

7. Numerical Simulation

In this section, we present numerical simulations that examine the sensitivity of key parameters with respect to the infected individuals and the dynamics of all population compartments to support analytical findings.

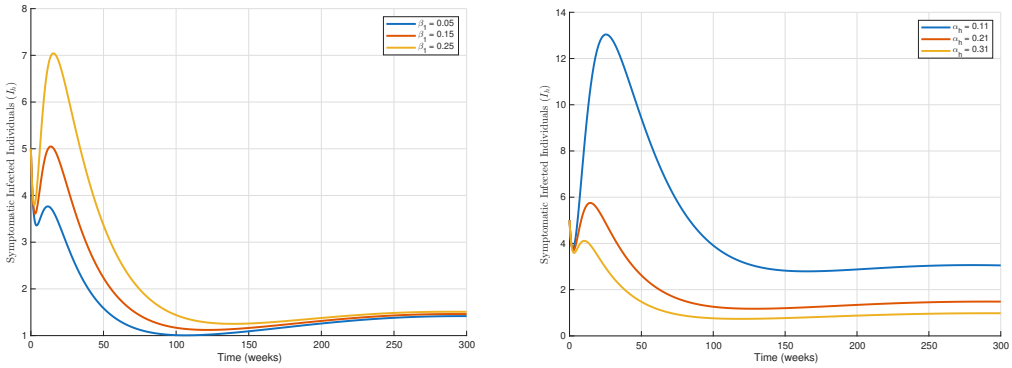

(a) (b)

Figure 6: Sensitivity of β_1 (panel (a)) and α_h (panel (b)) with respect to I_h.

Figure 6 displays the sensitivity of parameters β_1 and α_h with respect to symptomatic infected individuals (I_h). Panel (a) indicates that increasing β_1, the effective contact rate with asymptomatic individuals, yields

a higher transmission rate and a sharper infection peak. This means that a value of $\beta_1 = 0.25$ reaches the highest peak of infection around week 15 compared to $\beta_1 = 0.05$, which has a lower and slower peak. This result highlights the fact that a decrease in effective contact through non-pharmaceutical interventions such as social distancing or protection measures can significantly reduce the level of infection. Panel (b) indicates that increasing vaccination rate α_h significantly reduces the peak of symptomatic human infections. For example, while with $\alpha_h = 0.11$ the number of infected individuals rises to its peak around week 25, at $\alpha_h = 0.31$ the peak infection burden is much lower and declines more rapidly. These results suggest that vaccination coverage will successfully reduce the disease transmission and overall infection burden within the human population.

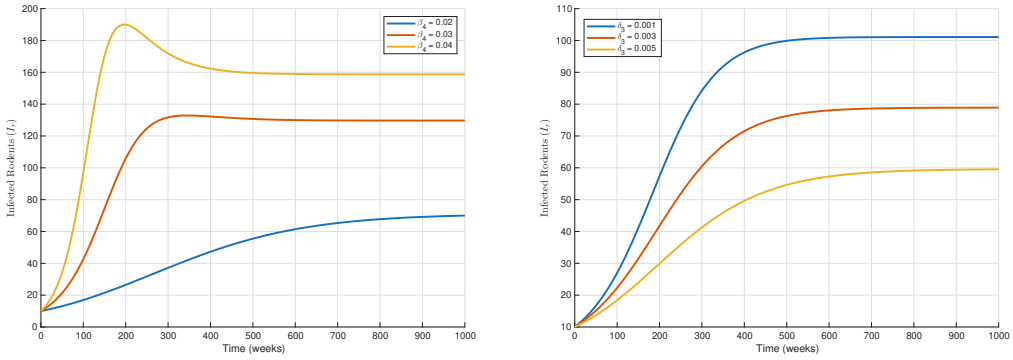

(a) (b)

Figure 7: Sensitivity of β_4 (panel (a)) and δ_3 (panel (b)) with respect to I_r.

Numerical simulations are carried out in Figure 7 to analyze parameters β_4 and δ_3 for sensitivity with respect to the infected rodents (I_r). An increase in β_4 directly accelerates the growth of the infected rodent population as depicted in panel (a). In this respect, for $\beta_4 = 0.04$, the infected rodent population increases rapidly and is close to 160 individuals at the end of the 1000 weeks of simulation, while for $\beta_4 = 0.02$, the increase in infections is slower. This indicates that controlling the contact rate among rodents, for example, by managing the reservoir population, can be used to limit the spread of the disease. The result in panel (b) indicates that an increased value of δ_3 dramatically delays the infected rodent population's growth. At $\delta_3 = 0.005$, the infected rodent population reaches a steady state at a level much lower than at $\delta_3 = 0.001$, where the population surges above 100. This behavior suggests that public health strategies aimed at increasing the mortality of infected rodents will be highly effective at reducing disease transmission.

In Figure 8, we present the numerical simulation of the dynamics of human and rodent populations in the Mpox transmission model for 500 weeks. This figure contains four panels, each with different dynamics of the model, due to the varying compartments, as well as the significant differences in the initial conditions. Panel (a) shows the dynamics of susceptible individuals (S_h) and vaccinated individuals (V_h). We can see that S_h rapidly declines in the first weeks due to infection transmission and vaccination efforts. This sharp decrease reflects the redistribution of S_h into both asymptomatic infected and vaccinated compartments. On the other hand, V_h grows rapidly in the early phase, as reflected by an effective vaccination rate. However, after reaching its peak, V_h gradually decreases, which can be attributed to natural death and transitions into the recovered compartment. This pattern suggests that vaccination contributes significantly to short-term epidemic mitigation. Panel (b) shows the time series of asymptomatic infected individuals (A_h) and symptomatic infected individuals (I_h). We can see that A_h reaches its peak at approximately week 10, indicating that silent transmission plays a dominant role during the early phase of the outbreak. The subsequent decline in A_h is mainly driven by transition to I_h and natural death. On the other hand, I_h is relatively low as compared with A_h, but it follows a stable trend throughout the observation period. This behavior highlights the epidemiological significance of asymptomatic carriers, who may sustain transmission without being easily detected. Panel (c) depicts the steadily growing numbers of recovered individuals (R_h). We can see that R_h grows quite suddenly and eventually becomes the majority of the total uninfected human population past

week 5 as humans move from V_h and I_h into this demographic. Panel (d) shows the dynamics of susceptible rodents (S_r) and infected rodents (I_r). We can see that S_r decreases smoothly over time, reflecting that part of this population becomes infected and thus moves into I_r. On the other hand, I_r increases at a relatively stable rate, which underlines the importance of rodents for the disease to persist as a reservoir. Unlike the human population, where vaccination significantly alter the dynamics, the rodent system lacks an immunization mechanism, allowing infection to persist more steadily.

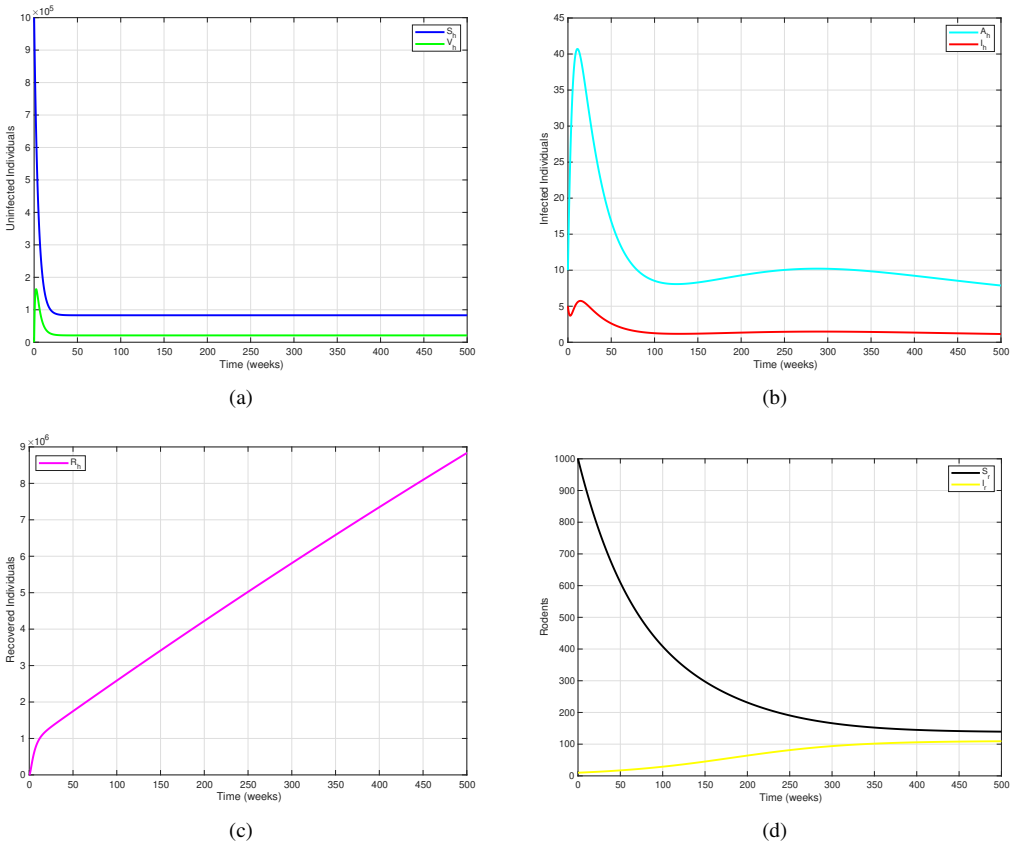

(a) (b) (c) (d)

Figure 8: Dynamics of human and rodent populations.

8. Conclusion

The transmission model of Mpox developed here involves asymptomatic individuals (A_h), alongside the following other compartments: susceptible individuals (S_h), vaccinated individuals (V_h), symptomatic infected individuals (I_h), recovered individuals (R_h), susceptible rodents (S_r), and infected rodents (I_r). By applying the contraction mapping principle, the model satisfies the well-posedness criteria, ensuring the existence, uniqueness, and stability of its solutions. Its solutions are also bounded and maintain non-negativity, confirming that the model is mathematically and epidemiologically consistent. Three equilibrium points are identified: the disease-free equilibrium (DFE), the human-endemic equilibrium (HEE) when the basic reproduction number of the human population ($\mathcal{R}_0^h$) is greater than one, and the endemic equilibrium (EE) when the basic reproduction number of the rodent population ($\mathcal{R}_0^r$) is greater than one. The DFE is both locally and globally asymptotically stable if the basic reproduction number ($\mathcal{R}_0$) is less than one. If they exist, the HEE is globally asymptotically stable if $\mathcal{R}_0^r$ is less than one and the EE is always globally asymptotically stable. Sensitivity analysis indicates that parameters β_1 and α_h are the most influential on

$\mathcal{R}_0^h$, where β_1 positively correlates, and α_h negatively correlates with $\mathcal{R}_0^h$. These results show that reducing the contact rate with asymptomatic individuals and increasing vaccination rate play a major role in lowering outbreak intensity. On the other hand, among the model parameters, β_4 and δ_3 have the highest influence on $\mathcal{R}_0^r$, where β_4 positively correlates, and δ_3 is negatively correlated with $\mathcal{R}_0^r$. These results highlight that controlling rodent-to-rodent contact rate and increasing rodent death rate due to Mpox significantly reduce the long-term persistence of the disease in the rodent population.

According to the results obtained by simulation, human and rodent parameters contribute much towards shaping the transmission dynamics. A higher value of β_1 increases human-to-human transmission, giving rise to a spikier peak of infection, whereas decreasing β_1, through non-pharmaceutical interventions such as social distancing and protective measures, significantly lowers the levels of infection. Vaccination also plays an imperative role. Increasing α_h suppresses the symptomatic infection peak and quickens its decline, showing that rapid vaccination coverage is critical for mitigating disease burdens. In addition, the infection transmission depends on rodent-related parameters such that a higher β_4 hastens the infections of rodents, while an increase in δ_3 effectively decreases the infected population of rodents, indicating the need for management of reservoirs and vector control. From compartmental dynamics, it follows that S_h declines because of both infection and vaccination, whereas V_h first increases and then decreases, dominated by R_h after approximately 5 weeks. In contrast, A_h reaches its peak in approximately week 10 and then slowly decreases, with I_h remaining low, yet rather stable, during the whole observation time. In contrast, I_r is growing steadily, while S_r steadily decreases over time, reflecting the ongoing infection. These results confirm that integrated strategies of vaccination, reduction of human contact, and management of the rodent population are required in order to control disease transmission and lower the overall infection burden. The proposed numerical simulation preserves the boundedness and non-negativity of solutions without requiring excessively small time steps, thereby ensuring biological feasibility throughout the simulation. Furthermore, it exhibits strong stability and effectively captures long-term dynamics, making it a reliable and efficient computational tool for simulating Mpox transmission systems.

However, this study has a number of limitations. The model is based on homogeneous mixing among individuals, as well as constant parameter values without environmental or behavioral variability that could better describe the complexity of real-world transmission. Rodent population dynamics and interspecies interactions are also simplified in such a way that potentially limits the ecological realism of the model. Future works may stress the incorporation of spatial heterogeneity and mobility patterns for representing Mpox spread across various regions. Also, the integration of stochastic effects, time-varying parameters, or even more detailed vaccination or age-structured strategies can add to the value of such a model for public health policy and planning of outbreak control.

ACKNOWLEDGMENT

The authors gratefully acknowledge the reviewers' constructive feedback and the editorial team's valuable support. The authors also acknowledge support by E+CBHE program through GREENSEA project Grant (No. 101232814).

REFERENCES

[1] Abidemi, A., Fatmawati and Peter, O.J., Deterministic double dose vaccination model of COVID-19 transmission dynamics: Optimal control strategies with cost-effectiveness analysis, Communication in Biomathematical Sciences, 7(1), pp. 1–33, 2024.

[2] Afolabi, Y.O. and Wade, B.A., Dynamics of transmission of a monkeypox epidemic in the presence of an imperfect vaccination, Results in Applied Mathematics, 19, p. 100391, 2023.

[3] Ahmad, A., Farman, M., Naik, P.A., Hincal, E., Iqbal, F. and Huang, Z., Bifurcation and theoretical analysis of a fractional-order Hepatitis B epidemic model incorporating different chronic stages of infection, Journal of Applied Mathematics and Computing, 71, pp. 1543–1564, 2025.

[4] Akinyemi, S.T., Idisi, I.O., Rabiu, M., Okeowo, V.I., Iheonu, N., Dansu, E.J., Abah, R.T., Mogbojuri, O.A., Audu, A.M., Yahaya, M.M., Ebimobowei, J.S., Akande, K.B., Ojoma, A.A., Adeniji, A.A. and Oshinubi, K., A tale of two countries: Optimal control and cost-effectiveness analysis of monkeypox disease in Germany and Nigeria, Healthcare Analytics, 4, p. 100258, 2023.

[5] Alakunle, E., Moens, U., Nchinda, G. and Okeke, M.I., Monkeypox virus in Nigeria: infection biology, epidemiology, and evolution, Viruses, 12(11), p. 1257, 2020.

[6] Al-Shomrani, M.M., Musa, S.S. and Yusuf, A., Unfolding the transmission dynamics of monkeypox virus: an epidemiological modelling analysis, Mathematics, 11(5), p. 1121, 2023.

[7] Bankuru, S.V., Kossol, S., Hou, W., Mahmoudi, P., Rychtář, J. and Taylor, D., A game-theoretic model of monkeypox to assess vaccination strategies, PeerJ, 8, p. e9272, 2020.

[8] Betti, M.I., Farrell, L. and Heffernan, J., A pair formation model with recovery: Application to Mpox, Epidemics, 44, p. 100693, 2023.

[9] Blase, W.I.C., Balsomo, A.J. and Sabinay, S.G., Modeling the co-infection dynamics of COVID-19 and dengue: Well-posedness, analysis of equilibrium properties and numerical simulations, Communication in Biomathematical Sciences, 7(2), pp. 177–201, 2024.

[10] Bonyah, E., Panigoro, H.S., Fatmawati, Rahmi, E. and Juga, M.L., Fractional stochastic modelling of monkeypox dynamics, Results in Control and Optimization, 12, p. 100277, 2023.

[11] Brauer, F. and Castillo-Chavez, C., Mathematical Models in Population Biology and Epidemiology, Springer-Verlag, 2011.

[12] Brauer, F., Castillo-Chavez, C. and Feng, Z., Mathematical Models in Epidemiology, Springer, 2019.

[13] Bragazzi, N.L., Han, Q., Iyaniwura, S.A., Omame, A., Shausan, A., Wang, X., Woldegerima, W.A., Wu, J. and Kong, J.D., Adaptive changes in sexual behavior in the high-risk population in response to human monkeypox transmission in Canada can help control the outbreak: Insights from a two-group, two-route epidemic model, Journal of Medical Virology, 95(4), p. e28575, 2023. https://doi.org/10.1002/jmv.28575

[14] CDC, About Monkeypox, 2025. https://www.cdc.gov/monkeypox/about/index.html, Accessed on July, 2025.

[15] CDC, How Monkeypox Spreads, 2025. https://www.cdc.gov/monkeypox/causes/index.html, Accessed on July, 2025.

[16] Chitnis, N., Hyman, J.M. and Cushing, J.M., Determining Important Parameters in the Spread of Malaria Through the Sensitivity Analysis of a Mathematical Model, Bulletin of Mathematical Biology, 70, pp. 1272-1296, 2008.

[17] Devi, A.S., Naik, P.A., Boulaaras, S., Sene, N. and Huang, Z., Understanding the transmission mechanism of HIV/TB co-infection using fractional framework with optimal control, International Journal of Numerical Modelling: Electronic Networks, Devices and Fields, 38(4), p. e70097, 2025.

[18] Diekmann, O., Heesterbeek, J.A.P. and Roberts, M.G., The construction of next-generation matrices for compartmental epidemic models, Journal of the Royal Society Interface, 7(47), pp. 873–885, 2010.

[19] Elsonbaty, A., Adel, W., Aldurayhim, A. and El-Mesady, A., Mathematical modeling and analysis of a novel monkeypox virus spread integrating imperfect vaccination and nonlinear incidence rates, Ain Shams Engineering Journal, 15, p. 102451, 2024.

[20] Fernandes, G.D. and Maldonado, V., Behavioral aspects and the transmission of monkeypox: A novel approach to determine the probability of transmission for sexually transmissible diseases, Infectious Disease Modelling, 8, pp. 842–854, 2023.

[21] Janan, T., Fatmawati, Alfiniyah, C., Martini, S., Aldila, D. and Hasan, A., Dynamical analysis and optimal control of the Mpox transmission model with stratified susceptibility, Mathematical Modelling and Numerical Simulation with Applications, 6(1), pp. 186-227, 2026.

[22] La Salle, J.P., The Stability of Dynamical Systems, SIAM, 1976.

[23] Li, S., Samreen, Ullah, S., AlQahtani, S.A., Tag, S.M. and Akgül, A., Mathematical assessment of monkeypox with asymptomatic infection: prediction and optimal control analysis with real data application, Results in Physics, 51, p. 106726, 2023.

[24] Martcheva, M., An Introduction to Mathematical Epidemiology, Springer: New York, 2015.

[25] Murray, J.D., Mathematical Biology: I. An Introduction, Springer, 2007.

[26] Musa, S.S., Yusuf, A., Bakare, E.A., Abdullahi, Z.U., Adamu, L., Mustapha, U.T. and He, D., Unravelling the dynamics of Lassa fever transmission with differential infectivity: Modeling analysis and control strategies, Mathematical Biosciences and Engineering, 19(12), pp. 13114–13136, 2022.

[27] Naidu, D.S., Optimal Control Systems, Taylor & Francis, 2002.

[28] Naik, P.A., Farman, M., Jamil, S., Saleem, M.U., Nisar, K.S. and Huang, Z., Modeling and computational study of cancer treatment with radiotherapy using real data, PLoS One, 20(5), p. e0320906, 2025.

[29] Naik, P.A., Yeolekar, B.M., Qureshi, S., Yeolekar, M. and Madzvamuse, A., Modeling and analysis of the fractional-order epidemic model to investigate mutual influence in HIV/HCV co-infection, Nonlinear Dynamics, 112(13), pp. 11679–11710, 2024.

[30] Ngungu, M., Addai, E., Adeniji, A., Adam, U.M. and Oshinubi, K., Mathematical epidemiological modeling and analysis of monkeypox dynamism with non-pharmaceutical intervention using real data from the United Kingdom, Frontiers in Public Health, 11, p. 1101436, 2023.

[31] Olaniyi, S. and Chuma, F.M., Lyapunov stability and economic analysis of monkeypox dynamics with vertical transmission and vaccination, International Journal of Applied and Computational Mathematics, 9(5), p. 85, 2023.

[32] Raffoul, Y.N., Advanced Differential Equations, Academic Press, 2023.

[33] Samreen, Ullah, S., Nawaz, R. and Alshehri, A., Mathematical modeling of monkeypox infection with optimized preventive control analysis: a case study with 2022 outbreak, European Physical Journal Plus, 138(8), p. 689, 2023.

[34] Sayarshad, H.R., Interventions in demand and supply sides for vaccine supply chain: An analysis on monkeypox vaccine, Operations Research Perspectives, 11, p. 100285, 2023.

[35] Somma, S.A., Akinwande, N.I. and Chado, U.D., A mathematical model of monkeypox virus transmission dynamics, Ife Journal of Science, 21(1), pp. 195–204, 2019.

[36] Strauss, W.A., Partial Differential Equations: An Introduction, Wiley, 2007.

[37] Thornhill, J.P., Barkati, S., Walmsley, S., Rockstroh, J., Antinori, A., Harrison, L.B., Palich, R., Nori, A., Reeves, I. and Habibi, M.S., Monkeypox virus infection in humans across 16 countries—April–June 2022, New England Journal of Medicine, 387(8), pp. 679–691, 2022.

[38] Usman, S. and Adamu, I.I., Modeling the transmission dynamics of the monkeypox virus infection with treatment and vaccination interventions, Journal of Applied Mathematics and Physics, 5(12), pp. 2335–2353, 2017.

[39] WHO, Mpox (monkeypox) outbreak 2022, 2022. https://www.who.int/emergency/situations/monkeypox-oubreak-2022, Accessed on July, 2025.

[40] WHO, Mpox, 2024. https://www.who.int/news-room/fact-sheets/detail/mpox, Accessed on July, 2025.

[41] WHO, Mpox, 2024. https://www.who.int/news-room/questions-and-answers/item/mpox, Accessed on July, 2025.

[42] WHO, WHO Director-General declares mpox outbreak a public health emergency of international concern, 2024. https://www.who.int/news/item/14-08-2024-who-director-general-declares-mpox-outbreak-a-public-health-emergency-of-international-concern, Accessed on July, 2025.

[43] Zhang, X.S., Mandal, S., Mohammed, H., Turner, C., Florence, I., Walker, J., Niyomsri, S., Amirthalingam, G., Ramsay, M., Charlett, A. and Vickerman, P., Transmission dynamics and effect of control measures on the 2022 outbreak of Mpox among gay, bisexual, and other men who have sex with men in England: A mathematical modelling study, Lancet Infectious Diseases, 24(1), pp. 65–74, 2024.